Published in final edited form as:
Am J Physiol Heart Circ Physiol. 2008 June ; 294(6): H2604–H2613. doi:10.1152/ajpheart.91506.2007.

Impaired relaxation is the main manifestation in transgenic mice expressing a restrictive cardiomyopathy mutation, R193H, in cardiac TnI

Jianfeng Du[1], **Jing Liu**[1], **Han-Zhong Feng**[2], **M. M. Hossain**[2], **Nariman Gobara**[1], **Chi Zhang**[1], **Yuejin Li**[1], **Pierre-Yves Jean-Charles**[1], **Jian-Ping Jin**[2], and **Xu-Pei Huang**[1]

[1]Department of Biomedical Science and Center for Molecular Biology and Biotechnology, University of Miami Miller School of Medicine Boca Regional Campus, Florida Atlantic University, Boca Raton, Florida

[2]Section of Molecular Cardiology, Evanston Northwestern Healthcare and Northwestern University Feinberg School of Medicine, Evanston, Illinois

Abstract

Transgenic mice were generated to express a restrictive cardiomyopathy (RCM) human cardiac troponin I (cTnI) R192H mutation in the heart (cTnI^{193His} mice). The objective of this study was to assess cardiac function during the development of diastolic dysfunction and to gain insight into the pathophysiological impact of the RCM cTnI mutation. Cardiac function and pathophysiological changes were monitored in cTnI^{193His} mice and wild-type littermates for a period of 12 mo. It progressed gradually from abnormal relaxation to diastolic dysfunction characterized with high-resolution echocardiography by a reversed E-to-A ratio, increased deceleration time, and prolonged isovolumetric relaxation time. At the age of 12 mo, cardiac output in cTnI^{193His} mice was significantly declined, and some transgenic mice showed congestive heart failure. The negative impact of cTnI^{193His} on ventricular contraction and relaxation was further demonstrated in isolated mouse working heart preparations. The main morphological change in cTnI^{193His} myocytes was shortened cell length. Dobutamine stimulation increased heart rate in cTnI^{193His} mice but did not improve CO. The cTnI^{193His} mice had a phenotype similar to that in human RCM patients carrying the cTnI mutation characterized morphologically by enlarged atria and restricted ventricles and functionally by diastolic dysfunction and diastolic heart failure. The results demonstrate a critical role of the COOH-terminal domain of cTnI in the diastolic function of cardiac muscle.

Keywords

troponin I; cardiac relaxation; Doppler echocardiography; working heart function

CARDIOMYOPATHIES ARE DISORDERS that primarily affect cardiac muscles and are associated with varying degrees of cardiac dysfunction. On the basis of morphology and pathophysiological changes, cardiomyopathies may be classified into three major subtypes: hypertrophic cardiomyopathy (HCM), dilated cardiomyopathy (DCM), and restrictive cardiomyopathy (RCM). Among these, RCM shows the worst prognosis. Some cardiomyopathies are now characterized as “sarcomeric diseases” on the basis of evidence that mutations in sarcomeric proteins are causal.

Address for reprint requests and other correspondence: X. Huang, Dept. of Biomedical Science, Florida Atlantic Univ., 777 Glades Rd., Boca Raton, FL 33431 (xhuang@fau.edu)..

Contractile sarcomeric protein mutations, truncations, or deletion have been identified for various cardiomyopathies in humans or experimental animals (17,23,27,38,41,43).

The cardiac sarcomere consists of a highly ordered assembly of myosin thick filaments, actin thin filaments, and associated proteins such as tropomyosin and troponin C, T, and I. Cardiac troponin I (cTnI) is the inhibitory subunit of the troponin complex, which binds to actin-tropomyosin and prevents muscle contraction by inhibition of actin-tropomyosin-activated myosin (actomyosin) ATPase (49). Many clinical and experimental studies have shown that TnI mutations are associated with HCM (19,22,31,42). Recently, a linkage study has, for the first time, demonstrated that idiopathic RCM can be a part of the clinical expression of cTnI mutation (30). A point mutation in the human cTnI gene results in an amino acid substitution (R192H in humans) in the COOH-terminal region of cTnI. It is important to note that the R192H mutation is located in the COOH-terminal region that is highly conserved and required for the full inhibitory action of cTnI (10,20,28). The first transgenic (TG) mouse model (cTnI^{193His} mice) carrying the RCM cTnI mutation (Arg193His in mouse cTnI protein, cTnI-R193H) was recently created in our laboratory (8). In preliminary studies, we reported (8) that the phenotype of the cTnI^{193His} mice is very similar to the clinical features of RCM patients carrying the same cTnI mutation. It includes dilated atria and a decreased left ventricular end-diastolic dimension (LVEDD) without significant changes in systolic function (8). However, the molecular mechanism underlying the cTnI mutation-caused RCM is still unknown. The cardiac function, in particular the diastolic function, in the TG mice expressing the RCM cTnI mutation remained to be characterized in order to understand the development of the disease and to find the earliest and most sensitive signs in the TG mice. In the present study, we used in vivo cardiac function measurements on cTnI^{193His} mice over a period of 12 mo and analyzed the effect of cTnI-R193H on cardiac function in TG mouse hearts, using ex vivo isolated working heart preparations. The results demonstrated that impaired relaxation and restrictive physiology are the main manifestations in TG mice carrying RCM TnI mutation characterized morphologically by enlarged atria and restricted ventricles and functionally by diastolic dysfunction and diastolic heart failure.

METHODS

RCM cTnI^{193His} transgenic mice

The mice used in this study were generated in our laboratory by transgenic expression of cTnI^{193His} mutant protein in the heart under the α-myosin heavy chain promoter and maintained as a pathogen-free colony at Florida Atlantic University at Boca Raton, FL. The transgenic construction and genotyping were described previously (8). Wild-type (WT) littermates were used as controls in the present study. This investigation conforms to the *Guide for the Care and Use of Laboratory Animals* (NIH Pub. No. 85–23, revised 1996) and was in accordance with the protocols approved by the Institutional Animal Care and Use Committees at Florida Atlantic University and Evanston Northwestern Healthcare.

Monoclonal anti-TnI antibodies

The mouse monoclonal antibody (MAb) TnI-1 was previously developed by immunization with purified chicken fast TnI (20). TnI-1 recognizes fast, slow, and cardiac TnIs at an epitope conserved in the COOH-terminal region (20).

MAb 4H6 was developed by immunization of the Balb/c mouse with a central fragment of mouse cTnI (amino acids 30–191) expressed in *Escherichia coli*. The purification of the cTnI30-191 fragment was carried out as described previously (2). Fusion with the SP2/0 myeloma cell line, hybridoma screening, and limiting dilution subclonings were performed as

described previously (20). Immunoglobulin isotyping determined that MAb 4H6 is an IgG2bκ.

SDS-PAGE and Western blotting

Whole cardiac muscle was homogenized in SDS-polyacrylamide gel electrophoresis (SDS-PAGE) sample buffer containing 2% SDS to extract myofilament proteins. The samples were resolved by 14% Laemmli SDS-PAGE with an acrylamide-to-bisacrylamide ratio of 180:1 and a Bio-Rad mini-Protean II system, and the protein bands were transferred to a nitrocellulose membrane with a Bio-Rad Lab semidry electrotransfer apparatus. The nitrocellulose membrane was blocked with 1% bovine serum albumin in Tris-buffered saline (TBS; 150 mM NaCl, 50 mM Tris·HCl, pH 7.5) and incubated with MAb TnI-1 against the COOH terminus of TnI (2) and MAb 4H6 against an epitope in the central region of TnI diluted in TBS containing 0.1% bovine serum albumin. The subsequent washes, incubation with alkaline phosphatase-labeled anti-mouse IgG second antibodies (Sigma), and 5-bromo-4-chloro-3-indolyl phosphate-nitro blue tetrazolium substrate reaction were carried out as described previously (2).

A double-transgenic mouse line (cTnI KO+R193H) was produced by crossbreeding of the cTnI-R193H TG mice with a cTnI gene knockout mouse line (18) to express the cTnI-R193H transgene on a cTnI gene knockout background. Similar to the cTnI gene knockout mice, the double-transgenic mice die 18 days after birth when slow TnI ceases expression in the heart, indicating a severe defect in the function of cTnI-R193H. Nonetheless, 16-day-old postnatal cardiac muscle samples from the double-transgenic mice were used in Western blotting to test the reactivity of the anti-cTnI MAbs against cTnI-R193H in the absence of wild-type cTnI.

Ser23/24 phosphorylation status of cTnI was determined in cardiac muscle samples from TG or WT mice by Western blotting using antibodies that detect the phosphorylated form of cTnI (Abcam, Cambridge, MA). Three WT and three TG mice were used to measure the cTnI basal phosphorylation status, and three WT and three TG mice were used to measure the cTnI phosphorylation status after dobutamine treatment (1.5 μg/g body wt ip). Myofibril proteins were isolated with a tissue homogenizer in a lysis buffer (mM: 100 KCl, 10 imidazole, 2 EGTA, 1 $MgCl_2$, pH 7.0) containing protease/phosphatase inhibitors (protease inhibitor cocktail and phosphatase inhibitor cocktail 2 from Sigma). To control for equal protein loading on the gels, cTnI MAbs (4H6) were used to quantify cTnI concentrations. Western blots were scanned at 600 dpi for densitometric quantification with NIH Image 1.61 software.

In vivo transthoracic cardiac imaging with echocardiography

All echocardiography measurements were performed according to the standards established in human echocardiography (9,37,40). A Vevo 770 High-Resolution In Vivo Imaging System (VisualSonics, Toronto, ON, Canada) was used to perform echocardiography studies as described previously (8,25).

Doppler echocardiography analysis in mice

As previously described, echocardiograph images were acquired in TG and WT mice with the use of a high-resolution (40 MHz) transducer with a digital ultrasonic system. Pulse Doppler images were collected with the apical four-chamber view to record the mitral Doppler flow spectra. The Doppler sample volume was placed at the center of the orifice and at the tip level of the valves for the highest velocities. However, for measurement of the left ventricular systolic and diastolic time intervals, the Doppler sample volume was moved slightly toward the left ventricular outflow tract to intersect with both the mitral inflow and the left ventricular outflow in the same recording. Pulse wave Doppler tissue imaging (DTI) was also performed on experimental animals by activating the DTI function in Vevo 770 echocardiography. Sample volume was measured at the septal side of the mitral annulus. Early (E′) and late (A′) diastolic

mitral annulus velocity and the ratio of E′ to A′ were determined. Both mitral pulse Doppler and DTI data were collected on six TG mice and six WT mice from the age of 2 mo to 12 mo. Data analysis was performed off-line with the use of a customized version of Vevo 770 Analytic Software.

Functional measurement of isolated working mouse hearts

Cardiac function of TG and WT mice was measured at 12 mo of age with Langendorff-Neely isolated working heart preparations as described previously (2,16) at various preloads from 5 to 20 mmHg and a constant afterload of 90 mmHg. Mice were injected intraperitoneally with 100 U heparin and anesthetized with intraperitoneal injection of 100 mg/kg pentobarbital. The thoracic cavity was opened by a transverse incision to access and rapidly isolate the heart. The aorta was cannulated with a modified 18-gauge needle previously primed with perfusion fluid to avoid coronary air emboli. Retrograde perfusion through the aorta was initiated within 3 min after the thoracic cavity was opened. The hearts were perfused with a modified Krebs-Henseleit bicarbonate buffer (mM: 118 NaCl, 4.7 KCl, 2.25 $CaCl_2$, 2.25 $MgSO_4$, 1.2 KH_2PO_4, 0.32 EGTA, 25 $NaHCO_3$,15 D-glucose, and 2 sodium pyruvate, pH 7.4) aerated with 95% O_2-5% CO_2 at 37°C. After the Langendorff perfusion was established, the pulmonary artery and veins were exposed by further dissections. A modified 16-gauge needle was used to cannulate the pulmonary vein and left atria. A 30-gauge needle was used to puncture the left ventricle wall via the apex for the insertion of a 1.2-Fr pressure-volume catheter (model 898B, Scisense, London, ON, Canada). Intra-left ventricular placement of the catheter was confirmed by the pressure and volume values recorded. The pulmonary artery was cannulated with PE-50 tubing to collect right ventricular output from coronary effluent.

The heart was then switched to the working mode by perfusion from the left atrium. Function of the isolated working hearts was measured at 37°C and 480 beats/min controlled by pacing through an isolated stimulator (World Precision Instrument, A365). Aortic flow and coronary effluent were measured in real time by counting drops with Chart software (AD Instruments, Colorado Springs, CO). The aortic pressure was measured with an MLT844 pressure transducer (Capto, Horten, Norway) attached to the aortic cannula. Heart rate, intraventricular pressure, maximum rate of left ventricle pressure development ($\pm dP/dt_{max}$), and left ventricle volume measurements were obtained through the calibrated pressure-volume catheter. The analog signal was amplified with an ML110 Bridge Amplifier (AD Instruments), sampled at 1,000 Hz by a Powerlab/16 SP digital data archiving system (AD Instruments), and stored on computer disk for subsequent analysis (2,16). Stroke volume (μl/mg heart tissue) was calculated as the sum of aortic flow and coronary effluent, normalized to heart rate. Time to peak pressure, time to 50% peak pressure, and relaxation time at 75% total relaxation were measured from the left ventricle pressure traces.

Morphology measurement of isolated cardiac myocytes

Cardiac myocytes were isolated from 10-mo-old TG and WT mice with a Langendorff perfusion cell isolation system (Cellutron). The myocytes were cultured in mouse myocyte culture medium provided by the same company, and cell length and width were measured immediately after isolation in viable myocytes with a clear striated sarcomere pattern with an Olympus IX 71 microscope; 150 myocytes from 4 separated TG or WT heart preparations were examined.

β-Adrenergic stress assays

For assessment of left ventricular systolic and diastolic dynamics, B-mode, M-mode, and Doppler echocardiography were performed at rest and after intraperitoneal bolus injection of the β-receptor agonist dobutamine (1.5 μg/g body wt). Assays were performed on five TG and five WT mice.

Statistics

All results are presented as means ± SE. ANOVA and Student's *t*-test were used to determine statistical significance. Statistical significance was set at $P < 0.05$.

RESULTS

To investigate the functional effect of cTnI-R193H, it is essential to estimate its incorporation level in TG mouse cardiac myofilaments. The SDS-PAGE mobility of the mutant protein cTnI-R193H is identical to that of the WT cTnI. However, the Western blot in Fig. 1*A* demonstrated that the cTnI-R193H mutation completely abolished the binding of MAb TnI-1, which is known to recognize a COOH-terminal epitope (20). Consistent with this, we showed previously (20) that the COOH-terminal truncated cTnI (1–192) (50) lost reactivity to TnI-1. Therefore, TnI-1 provides a useful tool in the quantification of cTnI-R193H overexpressed in TG mouse hearts.

By comparing the TnI-1 blot detecting only endogenous WT cTnI and the MAb 4H6 blot detecting both WT and cTnI-R193H, we determined the mutant cTnI replacement rate in TG mouse cardiac muscle. The 4H6 Western blots showed similar levels of total cTnI in the TG and control hearts, while the TnI-1 blot detected decreased levels of WT cTnI in the TG hearts due to the incorporation of $cTnI^{193His}$ (Fig. 1*B*). Densitometry of the Western blots showed that the replacement rate of mutant cTnI in $cTnI^{193His}$ cardiac myocytes is ~25–30% (Fig. 1*C*). This estimate is consistent with the results obtained from RT-PCR and two-dimensional gel measurements (8), and the confirmed mutant protein replacement rate in the TnI^{193His} TG mouse hearts is similar to that of a previously reported cTnI TG mouse model, $cTnI^{146Gly}$ (19).

The mortality rate of $cTnI^{193His}$ mice was monitored for a period of 14 mo, and it was higher than that of WT control mice. The survival rate in TG mice at age of 14 mo was ~70%, while no death was found in 15 WT mice at the same age (Fig. 2*A*). Autopsy examination revealed enlarged livers in some of the transgenic mice at 10 mo of age. However, neither significant hypertrophy nor ventricular dilation was detected in heart samples examined with histological assays (Fig. 2*B*).

B-mode and M-mode echocardiography observations on $cTnI^{193His}$ mice were very similar to those previously reported (8). Doppler examination of mitral inflow has been most widely used to evaluate left ventricular diastolic function. Because the mitral inflow velocity profile is affected by several other factors, it is desirable to have mitral annulus velocity determined by DTI as an additional measurement since DTI measurement is a relatively preload-independent variable in evaluating diastolic function (45). We applied both mitral pulse Doppler and DTI to examine the experimental animals from age 2 to 12 mo for cardiac function, in particular the left ventricular diastolic function as illustrated in Fig. 3, *A* and *B*, respectively.

Figure 4 shows typical images of mitral pulse Doppler and DTI in TG and WT mice. At the age of 4 mo, there were no significant differences in mitral inflow profiles and mitral annulus velocity between TG and WT mice (E/A: 1.8 ± 0.3 in WT vs. 1.2 ± 0.1 in TG; E′/A′: 1.5 ± 0.2 in WT vs. 1.1 ± 0.6 in TG). However, at 10 mo, the E-to-A velocity peak ratio was reversed in TG mice (1.7 ± 0.4 in WT vs. 0.9 ± 0.3 in TG, $P < 0.05$). A similar reverse in E′/A′ was also observed by DTI in TG mice (1.2 ± 0.1 in WT vs. 0.9 ± 0.2 in TG, $P < 0.05$), indicating an impaired relaxation in TG hearts (Fig. 4). At 12 mo, although mitral inflow in some TG mice showed a “normal” pattern, i.e., E peak value is larger than A peak value (E/A: 2.3 ± 0.9 in WT vs. 1.6 ± 0.5 in TG), DTI examination revealed a reduced peak E′ velocity and hence a reversed E′/A′ in the same mice (E′/A′: 1.4 ± 0.1 in WT vs. 0.8 ± 0.1 in TG, $P < 0.05$) (Fig. 4). The data from pulse Doppler and DTI on 12-mo-old TG mice revealed a pseudonormalization pattern with diastolic dysfunction.

The mitral annulus velocity profile has been reported in patients with RCM associating with a decrease in E′ and A′ (11,45). Hence, measurement of early mitral annulus velocity by DTI is a useful tool to distinguish normal diastolic pattern from pseudonormal and restrictive patterns (Fig. 5). The reduced E/A indicated that the early ventricular filling phase was more sensitive to the impaired ventricular relaxation, whereas the later filling phase assisted by atrial contraction was less affected by the cTnI-R193H mutation. The deceleration time (DT) of early mitral flow was prolonged significantly in $cTnI^{193His}$ mice starting at age of 6 mo and lasting to 12 mo of age, indicating impaired left ventricular relaxation resulting in diastolic dysfunction (Fig. 6*D*). Interestingly, isovolumetric contraction time (IVCT), defined as the interval between mitral valve closure and aortic valve opening, was not changed significantly in TG and WT mice throughout the 12-mo period of our study (Fig. 6*A*), whereas isovolumetric relaxation time (IVRT), defined as the interval between aortic valve closure and mitral valve opening, was significantly prolonged in TG mice starting at age of 4 mo (Fig. 6*B*). The data indicate that decreased LVEDD and prolonged IVRT are the first signs in $cTnI^{193His}$ hearts. This is consistent with previous reports demonstrating that IVRT is the most sensitive Doppler index to detect impaired relaxation because it is first to become abnormal (11,12). Cardiac output (CO) did not show significant change in TG mice until the age of 12 mo (Fig. 6*C*), consistent with the changes in ejection fraction (Table 1).

To further evaluate the effect of cTnI-R193H on myocardial function in the absence of neurohumoral influences, isolated working heart function was measured at 90-mmHg afterload and preloads of 5, 8, 10, 12.5, 15, and 20 mmHg. The 12-mo-old TG mouse hearts showed a tendency of decreased stroke volume (Fig. 7*A*). The data in Fig. 7*B* further showed a reduced response of the left ventricular end-diastolic volume (EDV) in the TG hearts to increases in preload. To quantitatively demonstrate the impaired contraction as well as relaxation of the $cTnI^{193His}$ hearts, the data summarized in Fig. 7, *C–E*, revealed that compared with WT controls the TG hearts had decreased contractile and relaxation velocities and prolonged systolic and diastolic time parameters. It is worth noting that the TG hearts had less increase in left ventricular EDV and stroke volume compared with WT hearts in response to increases in preload, suggesting a reduced cardiac compliance (Fig. 7, *A* and *B*). The functional data obtained in isolated ex vivo working hearts are consistent with the results obtained from the in vivo echocardiography measurements.

On the basis of the functional characterization, the impaired relaxation and restrictive physiology are the main manifestations in transgenic mice carrying the TnI-R193H mutation. Consistent with this, cardiac myocyte morphology under relaxing conditions indicated that the cardiac myocytes isolated from $cTnI^{193His}$ mice were 17% shorter but 15% wider compared with the myocytes from WT mice at the same age ($P < 0.05$) (Fig. 8, *A* and *B*). This result is consistent with the data from cultured myocytes carrying the cTnI-R193H mutation, suggesting a higher basal tone in the myocytes containing cTnI-R193H (7).

To assess whether changes in cTnI phosphorylation are associated with the relaxation impairment in $cTnI^{193His}$ mice, we examined Ser23/24 phosphorylation in cTnI, which has been reported to play a major role in regulation of cardiac myofilament calcium sensitivity and relaxation (46). Although phosphorylation levels of cTnI at Ser23/24 were significantly increased after dobutamine stimulation (155 ± 7% in WT + dobutamine vs. 100 ± 9% in WT without dobutamine, 161 ± 8% in TG + dobutamine vs. 102 ± 5% in TG without dobutamine; both $P < 0.05$), there were no significant changes either in basal phosphorylation level or in dobutamine-stimulated phosphorylation level between TG and WT mice (Fig. 8, *C* and *D*). The results indicate that impaired relaxation and prolonged IVRT and DT in left ventricles of TG mice are not associated with phosphorylation of cTnI at Ser23/24.

We further examined the effect of β-agonist stimulation on left ventricular systolic and diastolic dynamics. The results demonstrated that dobutamine administration induced a significant increase in heart rate in both TG and WT mice (Fig. 9*A*). CO was elevated significantly in WT mice on dobutamine stimulation, in parallel with the increase of heart rate. In contrast, CO was not changed in TG mice after dobutamine administration (Fig. 9*B*). In the RCM cTnI^{His193} mice, left ventricular end-systolic volume (ESV) did not change whereas left ventricular EDV decreased significantly at age of 12 mo compared with WT mice at the same age (Fig. 9, *C* and *D*). This contributes to the decreased stroke volume that equals to EDV minus ESV. Dobutamine-stress increased cardiac contractility and decreased ESV in both WT and TG mice (Fig. 9*D*). While the treatment had little effect on EDV of WT mice, it significantly decreased EDV in TG mice (Fig. 9*C*).

DISCUSSION

We have generated a transgenic mouse model expressing the human RCM cTnI R192H mutation in adult cardiac muscle. The phenotype manifested in the cTnI^{193His} mice is very similar to that observed in RCM patients carrying the same mutation (30). Morphologically, the most dramatic change in cTnI^{193His} mice is ventricular restriction with decreased LVEDD due to shortened myocyte length. Functionally, the most significant changes are impaired relaxation manifested by prolonged IVRT and DT and restrictive physiology manifested by a reduced peak E′ velocity and hence a reversed E′/A′ on DTI. These data indicate that cTnI^{193His} mice provide a useful disease model for the study of human RCM. On the basis of longitudinal echocardiography investigation, the earliest signs in the RCM mice are the prolonged IVRT and restricted ventricles that start at age of 4 mo. It is also clear that no significant change of IVCT was detected in TG mice even at the age of 12 mo.

Doppler echocardiography has emerged as an important clinical tool to provide reliable and useful data for diastolic performance (6,15). The noninvasive nature and high-resolution feature of Vevo 770 echocardiography allow us to longitudinally monitor heart function in mice, so it is commonly used to obtain detailed phenotypic assessment for understanding the functional impact in genetically altered mouse models (1,8,47,53,54). From 12 mo of investigation, we demonstrated the pathophysiological development in the heart in RCM cTnI^{193His} mice, which progresses initially from abnormal relaxation gradually to diastolic dysfunction, and eventually to diastolic heart failure. The transmitral velocity pattern is the starting point of echocardiography assessment of left ventricular diastolic function, since it is easy to acquire and can rapidly distinguish normal from abnormal diastolic function in mice by E/A (early to late filling velocity ratio) (11,12,45). When relaxation impairs, early diastolic filling decreases progressively and a vigorous compensatory atrial contraction, i.e., atrial kick, occurs (Fig. 4). This results in a reversed E/A, increased DT, and prolonged IVRT (Fig. 7). It is observed that with disease progression left ventricular compliance becomes reduced and filling pressure begins to increase, leading to compensatory elevation of left atrial pressure with increase in early filling, so that the filling pattern looks relatively normal on 12-mo-old TG mice (pseudonormalization pattern, E/A > 1). In such cases, DTI is very useful to distinguish the pseudonormalization pattern from the normal filling pattern. Significantly decreased peak E′ velocity and E′/A′ < 1 in mitral annulus velocity define the pseudonormalization pattern with diastolic dysfunction. It should be pointed out that although the low concentration of isoflurane (~1.5%) that is used to anesthetize the mice for stable data acquisition is thought to have minimal effects on ventricular diastolic function in mice (53), the heart rate at this condition is ~450 beats/min, which is lower than that under conscious conditions. It is critical to apply the same conditions to both TG and WT experimental animals since the reduced heart rate may alter chamber size measurement.

The mortality rate in cTnI^{193His} mice is higher than that in their WT littermates. The cause of death is not clear, although some of the mice showed heart failure signs such as difficult breathing before death and some had an enlarged liver detected in autopsy. We found that 4 among 10 TG mice analyzed suffered from various degrees of enlarged liver. All of them were at ages of 10–12 mo. Hepatomegaly has been clinically reported in human patients suffering from RCM (4,5). Our data suggest that cTnI mutation-caused diastolic dysfunction could result in right-sided heart failure in aged TG mice. Although no significant abnormality in ECG was found in TG mice during echocardiography examinations, we did find some ECG changes in some TG mice. It will be useful to further analyze ECG changes in TG mice in future studies. Impaired relaxation is the main manifestation in cTnI^{193His} mice.

What is the mechanism underlying the damaged relaxation in myocytes carrying the cTnI-R193H mutation? An in vitro study using isolated rat cardiac myocytes infected with a recombinant adenovirus vector carrying the cTnI-R193H mutation reported that myofilaments incorporated with cTnI-R193H have a higher isometric tension than control myocytes at submaximal Ca^{2+} concentration ([Ca^{2+}]) and cTnI-R193H causes a Ca^{2+}-independent shortening of resting sarcomere length and slows relaxation (7). Both the in vitro study and our in vivo study found that the cell length was shorter in cardiac myocytes carrying the RCM cTnI mutation. The shortening of cardiac myocytes is caused by the increased basal mechanical tone without associated alteration in diastolic [Ca^{2+}], i.e., RCM cTnI-R193H causes a calcium-independent shortening of resting sarcomere length (7). In addition, our present study also revealed that phosphorylation levels in cTnI at Ser23/24 were not changed in RCM cTnI-R193H compared with WT. Dobutamine can cause an increase of cTnI phosphorylation in both WT and TG mouse hearts. Interestingly, dobutamine stress can also cause a significant increase of heart rate in cTnI^{193His} mice similar to that in WT control mice but did not increase CO as it did in WT mice, suggesting that the RCM cTnI^{193His} hearts are able to respond to β-adrenergic signaling but CO fails to increase in response to dobutamine stimulation because of the increased diastolic tone. The decreased capacity for stress response may explain the higher mortality in RCM cTnI^{193His} mice, although the penetration of the phenotypes of RCM cTnI R193H mutation in TG mice would depend on the combination of genetic and environmental factors as seen in RCM patients (30). No significant changes have been observed in Ca^{2+} transient and Ca^{2+} cycle-related proteins [Na^+/Ca^{2+} exchanger (NCX), sarco(endo) plasmic reticulum Ca^{2+}-ATPase (SERCA), PLB] in myocytes incorporated with cTnI-R193H mutants (7). Further studies are needed to explore the Ca^{2+} cycling changes with age in myocytes from cTnI^{193His} mice.

Many studies have demonstrated the functional consequences of troponin mutations linked to HCM, DCM, or RCM and have shown that these mutations alter the regulatory properties of troponin complex, resulting in an increase or a decrease in Ca^{2+} sensitivity of force generation that may primarily contribute to the pathogenesis of cardiomyopathies (14,21,26,29,33–36, 44,48). Very interestingly, different mutations in the same TnI molecule can result in HCM or RCM, i.e., TnI HCM mutations (R145G, R145Q, R162W, G203S, K206Q) and TnI RCM mutations (L144Q, R145W, A171T, K178E, D190G, R192H). It is still unknown how HCM or RCM mutations are manifested in vastly distinct diseases. It may be possible that clinical diagnostic techniques lack the ability to differentiate subtleties that exist between these two diseases (35). The other explanation could be that the different mutations have a direct effect on troponin function, since RCM mutations have been found to have much greater Ca^{2+}-sensitizing effects on force generation than TnI HCM mutations and structural changes have been observed in TnI RCM mutations (52).

Among the three major types of cardiomyopathy, RCM is the most malignant and the least studied (39). Most RCM patients eventually progress to overt heart failure (13,32). Clinically most RCM cases are idiopathic with unknown causes. Targeted activation of p38 MAP kinase

in ventricular myocytes resulted in a RCM in transgenic mice (24). The MAP kinase caused a severe RCM and premature death at 7–9 wk. The transgenic hearts exhibited marked interstitial fibrosis and expression of fetal marker genes characteristic of cardiac failure (24). Since stress-induced MAP p38 is activated in various forms of heart failure, it should be interesting to examine p38 MAP kinase activities in cardiac myocytes from cTnI^{193His} mice at the late stages with heart failure signs. However, the molecular mechanism underlying TnI mutation-caused RCM is different from the RCM caused by overactivated MAP kinases. A recent in vitro study on RCM cTnI-R193H mutant myocytes indicates that events downstream of Ca^{2+} handling are causal for the RCM cTnI-R193H defects and the thin filament is a unique target for possible therapeutic intervention (7). Hence, the RCM cTnI-R193H mutant mouse model investigated in the present study provides us with a useful tool for studies aimed at the treatment and prevention of myofibril protein mutation-caused RCM in humans.

Acknowledgments

GRANTS This work was supported by grants from the National Institutes of Health (GM-073621 to X.-P. Huang and HL-078773 to J.-P. Jin) and the American Heart Association (AHA) Florida/Puerto Rico Affiliate and from the Center of Excellence for Biomedical and Marine Biotechnology at Florida Atlantic University (to X.-P. Huang). J. Du is a recipient of a Predoctoral Fellowship Award from AHA Florida/Puerto Rico Affiliate.

REFERENCES

1. Appleton CP, Hatle LK, Popp RL. Relation of transmitral flow velocity patterns to left ventricular diastolic function: new insights from a com- bined hemodynamic and Doppler echocardiographic study. J Am Coll Cardiol 1988;12:426–440. [PubMed: 3392336]
2. Barbato J, Huang QQ, Hossain MM, Bond M, Jin JP. Proteolytic N-terminal truncation of cardiac troponin I enhances ventricular diastolic function. J Biol Chem 2005;280:6602–6609. [PubMed: 15611140]
3. Biesiadecki B, Jin JP. Exon skipping in cardiac troponin T of turkeys with inherited dilated cardiomyopathy. J Biol Chem 2002;277:18459–18468. [PubMed: 11886865]
4. Bilgic A, Ozbarlas N, Ozkutlu S, Ozer S, Ozme S. Cardiomyopathies in children. Clinical, epidemiological and prognostic evaluation. Jpn Heart J 1990;31:789–797. [PubMed: 2084276]
5. Chinnaiyan KM, Leff CB, Marsalese DL. Constrictive pericarditis versus restrictive cardiomyopathy: challenges in diagnosis and management. Cardiol Rev 2004;12:314–320. [PubMed: 15476569]
6. Collins KA, Korcarz CE, Lang RM. Use of echocardiography for the phenotypic assessment of genetically altered mice. Physiol Genomics 2003;13:227–239. [PubMed: 12746467]
7. Davis J, Wen H, Edwards T, Metzger JM. Thin filament disinhibition by restrictive cardiomyopathy mutant R193H troponin I induces Ca^{2+}-independent mechanical tone and acute myocyte remodeling. Circ Res 2007;100:1494–1502. [PubMed: 17463320]
8. Du J, Zhang C, Liu J, Sidky C, Huang XP. A point mutation (R192H) in the C-terminus of human cardiac troponin I causes diastolic dysfunction in transgenic mice. Arch Biochem Biophys 2006;456:143–150. [PubMed: 17027633]
9. Feigenbaum, H.; Armstrong, WF.; Ryan, T. Feigenbaum's Echocardiography. Vol. 6th ed.. Lippincott Williams & Wilkins; Philadelphia, PA: 2005. Evaluation of systolic and diastolic function of the left ventricle; p. 138-180.
10. Foster DB, Noguchi T, VanBuren P, Murphy AM, Van Eyk JE. C-terminal truncation of cardiac troponin I causes divergent effects on ATPase and force: implications for the pathophysiology of myocardial stunning. Circ Res 2003;93:917–924. [PubMed: 14551240]
11. Garcia MJ, Rodriguez L, Ares M, Griffin BP, Thomas JD. Differentiation of constrictive pericarditis from restrictive cardiomyopathy: assessment of left ventricular diastolic velocities in longitudinal axis by Doppler tissue imaging. J Am Coll Cardiol 1996;27:108–114. [PubMed: 8522683]
12. Giannuzzi P, Imparato A, Temporelli PL, de Vito F, Silva PL, Scapellato F, Giodano A. Doppler-derived mitral deceleration time of early filling as a strong predictor of pulmonary capillary wedge

pressure in postinfarction patients with left ventricular systolic dysfunction. J Am Coll Cardiol 1994;23:1630–1637. [PubMed: 8195524]

13. Hirota Y, Shimizu G, Kita Y, Nakayama Y, Suwa M, Kawamura K, Nagate S, Sawayama T, Izumi T, Nakano T. Spectrum of restrictive cardiomyopathy: report of the national survey in Japan. Am Heart J 1990;120:188–194. [PubMed: 2360503]
14. Ho CY, Seidman CE. A contemporary approach to hypertrophic cardiomyopathy. Circulation 2006;113:e858–e862. [PubMed: 16785342]
15. Ho CY, Sweitzer NK, McDonough B, Marron BJ, Casey SA, Seidman JG, Seidman CE, Solomon SD. Assessment of diastolic function with Doppler tissue imaging to predict genotype in preclinical hypertrophic cardiomyopathy. Circulation 2002;105:2992–2997. [PubMed: 12081993]
16. Huang QQ, Feng H, Liu J, Du J, Stull LB, Moravec C, Huang XP, Jin JP. Coexpression of skeletal and cardiac troponin T decreases mouse cardiac function. Am J Physiol Cell Physiol 2008;294:C213–C222. [PubMed: 17959729]
17. Huang XP, Du J. Troponin I, cardiac diastolic dysfunction and restrictive cardiomyopathy. Acta Pharmacol Sin 2004;25:1569–1575. [PubMed: 15569399]
18. Huang XP, Pi Y, Lee KJ, Henkel AS, Gregg RG, Powers PA, Walker JW. Cardiac troponin I gene knockout, a mouse model of myocardial troponin I deficiency. Circ Res 1999;84:1–8. [PubMed: 9915769]
19. James J, Zhang Y, Osinska H, Sanbe A, Klevitsky R, Hewett TE, Robbins J. Transgenic modeling of a cardiac troponin I mutation linked to familial hypertrophic cardiomyopathy. Circ Res 2000;87:805–811. [PubMed: 11055985]
20. Jin JP, Yang FW, Yu ZB, Ruse CI, Bond M, Chen A. The highly conserved COOH-terminus of troponin I forms a Ca^{2+}-modulated allosteric domain in the troponin complex. Biochemistry 2001;40:2623–2631. [PubMed: 11327886]
21. Kaski JP, Burch M, Elliott PM. Mutations in the cardiac troponin C gene are a cause of idiopathic dilated cardiomyopathy in childhood. Cardiol Young 2007;17:675–677. [PubMed: 17977476]
22. Kimura A, Harada H, Park JE, Hishi H, Satoh M, Takahashi M, Hiroi S, Sasaoka T, Ohbuchi N, Nakamura T, Koyanagi T, Hwang TH, Choo JA, Chung KS, Hasegawa A, Nagai R, Okazaki O, Nakamura H, Matsuzaki M, Sakamoto T, Toshima H, Koga Y, Imaizumi T, Sasazuki T. Mutations in the cardiac troponin I gene associated with hypertrophic cardiomyopathy. Nat Genet 1997;16:379–382. [PubMed: 9241277]
23. Kokado H, Shimizu M, Yoshio H, Ino H, Okeie K, Emoto Y, Matsuyama T, Yamaguchi M, Yasuda T, Fujino N, Ito H, Mabuchi H. Clinical features of hypertrophic cardiomyopathy caused by a Lys183 deletion mutation in the cardiac troponin I gene. Circulation 2000;102:663–669. [PubMed: 10931807]
24. Liao P, Geogakopoulos D, Kovacs A, Zheng M, Lerner D, Pu H, Saffitz J, Chien K, Xiao RP, Kass DA, Wang Y. The in vivo role of p38 MAP kinases in cardiac remodeling and restrictive cardiomyopathy. Proc Natl Acad Sci USA 2001;98:12283–12288. [PubMed: 11593045]
25. Liu J, Du J, Zhang C, Walker JW, Huang XP. Progressive troponin I loss impairs cardiac relaxation and causes heart failure in mice. Am J Physiol Heart Circ Physiol 2007;293:H1273–H1281. [PubMed: 17526646]
26. Lu QW, Morimoto S, Harada K, Du CK, Takahashi-Yanaga F, Miwa Y, Sasaguri T, Ohtsuki I. Cardiac troponin T mutation R141W found in dilated cardiomyopathy stabilizes the troponin T-tropomyosin interaction and causes a Ca^{2+} desensitization. J Mol Cell Cardiol 2003;35:1421–1427. [PubMed: 14654368]
27. Marian AJ, Roberts R. The molecular genetic basis for hypertrophic cardiomyopathy. J Mol Cell Cardiol 2001;33:655–670. [PubMed: 11273720]
28. Metzger JM, Westfall MV. Covalent and noncovalent modification of thin filament action: the essential role of troponin in cardiac muscle regulation. Circ Res 2004;94:146–158. [PubMed: 14764650]
29. Mogensen J. Troponin mutations in cardiomyopathies. Adv Exp Med Biol 2007;592:201–226. [PubMed: 17278367]

30. Mogensen J, Kubo T, Duque M, Uribe W, Shaw A, Murphy R, Gimeno JR, Elliott P, McKenna WJ. Idiopathic restrictive cardiomyopathy is part of the clinical expression of cardiac troponin I mutation. J Clin Invest 2003;111:209–216. [PubMed: 12531876]
31. Morner S, Richard P, Kazzam E, Hainque B, Schwartz K, Waldenstrom A. Deletion in the cardiac troponin I gene in a family from northern Sweden with hypertrophic cardiomyopathy. J Mol Cell Cardiol 2000;32:521–525. [PubMed: 10731450]
32. Nacruth R, Barretto AC, Mady C, Da Luz PL, Pileggi F. Idiopathic restrictive cardiomyopathy. Arq Bras Cardiol 1993;61:175–180. [PubMed: 8110048]
33. Ohtsuki I. Troponin: structure, function and dysfunction. Adv Exp Med Biol 2007;592:21–36. [PubMed: 17278353]
34. Peddy SB, Vricella LA, Crosson JE, Oswald GL, Cohn RD, Cameron DE, Valle D, Loeys BL. Infantile restrictive cardiomyopathy resulting from a mutation in the cardiac troponin T gene. Pediatrics 2006;117:1830–1833. [PubMed: 16651346]
35. Pinto JR, Parvatiyar MS, Jones MA, Liang J, Potter JD. A troponin T mutation that causes infantile restrictive cardiomyopathy increases Ca^{2+} sensitivity of force development and impairs the inhibitory properties of troponin. J Biol Chem 2007;283:2156–2166. [PubMed: 18032382]
36. Preston LC, Watkins H, Redwood CS. A revised method of troponin exchange in permeabilised cardiac trabeculae using vanadate: functional consequences of a HCM-causing mutation in troponin I. J Muscle Res Cell Motil 2006;27:585–590. [PubMed: 17051347]
37. Quinones MA, Otto CM, Stoddard M, Waggoner A, Zoghbi WA. Recommendations for quantification of Doppler echocardiography: a report from the Doppler Quantification Task Force of the Nomenclature and Standards Committee of the American Society of Echocardiography. J Am Soc Echocardiogr 2002;15:167–184. [PubMed: 11836492]
38. Redwood CS, Moolman-Smook JC, Watkins H. Properties of mutant contractile proteins that cause hypertrophic cardiomyopathy. Cardiovasc Res 1999;44:20–36. [PubMed: 10615387]
39. Rivenes SM, Kerrney DL, Smith EO, Towbin JA, Denfield SW. Sudden death and cardiovascular collapse in children with restrictive cardiomyopathy. Circulation 2000;102:876–882. [PubMed: 10952956]
40. Sahn DJ, DeMaria A, Kisslo J, Weyman A. Recommendations regarding quantitation in M-mode echocardiography: results of a survey of echocardiographic measurements. Circulation 1978;58:1072–1083. [PubMed: 709763]
41. Sanbe A, Nelson D, Gulick J, Setser E, Osinska H, Wang X, Hewett TE, Klevitsky R, Hayes E, Warshaw DM, Robbins J. In vivo analysis of an essential myosin light chain mutation linked to familial hypertrophic cardiomyopathy. Circ Res 2000;87:296–302. [PubMed: 10948063]
42. Sanbe A, James J, Tuzcu V, Nas S, Martin L, Gulick J, Osinska H, Sakthivel S, Klevitsky R, Ginsburg KS, Bers DM, Zinman B, Lakatta EG, Robbins J. Transgenic rabbit model for human troponin I-based hypertrophic cardiomyopathy. Circulation 2005;111:2330–2338. [PubMed: 15867176]
43. Seidman JG, Seidman C. The genetic basis for cardiomyopathy from mutation identification to mechanistic paradigm. Cell 2001;104:557–567. [PubMed: 11239412]
44. Sirenko SG, Potter JD, Knollmann BC. Different effect of troponin T mutations on the inotropic responsiveness of mouse hearts—role of myofilament Ca^{2+} sensitivity increase. J Physiol 2006;15:201–213. [PubMed: 16777946]
45. Sohn DW, Chai IH, Lee DJ, Kim HC, Kim HS, Oh BH, Lee MM, Park YB, Choi YS, Seo JD, Lee YW. Assessment of mitral annulus velocity by Doppler tissue imaging in the evaluation of left ventricular diastolic function. J Am Coll Cardiol 1997;30:474–480. [PubMed: 9247521]
46. Solaro, RJ. In Handbook of Physiology. The Cardiovascular System. The Heart. Vol. vol 1. Am Physiol Soc; Bethesda, MD: 2001. Modulation of cardiac myofilament activity by protein phosphorylation; p. 264-300.sect 2
47. Srinivasan S, Baldwin HS, Aristizabal O, Kwee L, Labow M, Artman M, Turnbull DH. Noninvasive, in utero imaging of mouse embryonic heart development with 40-MHz echocardiography. Circulation 1998;98:912–918. [PubMed: 9738647]
48. Takahashi-Yanaga F, Morimoto S, Harada K, Minakami R, Shiraishi F, Ohta M, Lu QW, Sasaguri I, Ohtsuki I. Functional consequences of the mutations in human cardiac troponin I gene found in familial hypertrophic cardiomyopathy. J Mol Cell Cardiol 2002;3:2095–2107.

49. Tobacman LS. Thin filament-mediated regulation of cardiac contraction. Annu Rev Physiol 1996;58:447–481. [PubMed: 8815803]
50. Van Eyk JE, Powers F, Law W, Larue C, Hodges RS, Solaro RJ. Breakdown and release of myofilament proteins during ischemia and ischemia/reperfusion in rat hearts: identification of degradation products and effects on the pCa-force relation. Circ Res 1998;82:261–271. [PubMed: 9468197]
51. Yanaga F, Morimoto S, Ohtsuki I. Ca^{2+}-sensitization and potentialation of the maximum level of myofibrillar ATPase activity caused by mutations of troponin T found in familial hypertrophic cardiomyopathy. J Biol Chem 1999;274:8806–8812. [PubMed: 10085122]
52. Yumoto F, Lu QW, Morimoto S, Tanaka H, Kono N, Nagata K, Ojima T, Takahashi-Yanaga F, Miwa Y, Sasaguri T, Nishita K, Tanokura M, Ohtsuki I. Drastic Ca^{2+} sensitization of myofilament associated with a small structural change in troponin I in inherited restrictive cardiomyopathy. Biochem Biophys Res Commun 2005;338:1519–1526. [PubMed: 16288990]
53. Zhou YQ, Foster FS, Parkes R, Adamson SL. Developmental changes in left and right ventricular diastolic filling patterns in mice. Am J Physiol Heart Circ Physiol 2003;285:H1563–H1575. [PubMed: 12805021]
54. Zhou YQ, Zhu Y, Bishop J, Davidson L, Henkelman RM, Bruneau BG, Foster FS. Abnormal cardiac inflow patterns during postnatal development in a mouse model of Holt-Oran syndrome. Am J Physiol Heart Circ Physiol 2005;289:H992–H1001. [PubMed: 15849237]

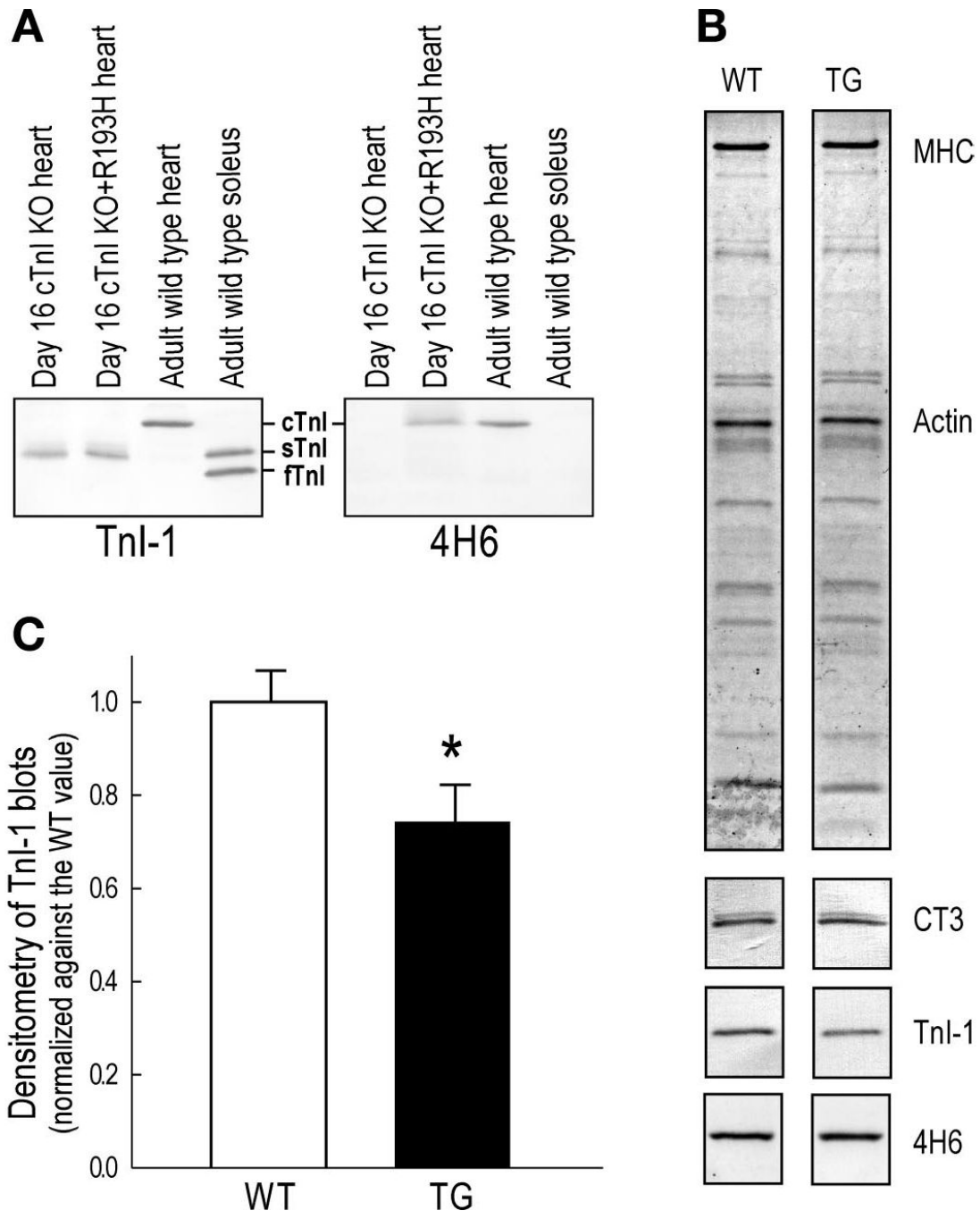

Fig. 1.

Expression of cardiac troponin I (cTnI)-R193H in transgenic (TG) mouse hearts. *A*: Western blots showed that whereas MAb 4H6 against an epitope in the central region of cTnI polypeptide recognized both wild-type (WT) cTnI and cTnI-R193H, MAb TnI-1 against the COOH terminus of TnI recognized only WT cTnI but not cTnI-R193H expressed on an endogenous cTnI knockout (KO) background. The expression of slow TnI in the 16-day-old cardiac muscle was detectable by MAb TnI-1 but not 4H6, consistent with 4H6's specificity to cTnI as shown by its lack of reaction to slow and fast TnIs in the soleus muscle. *B*: SDS-PAGE and Western blots showed that while the overall protein profile and the level of total cTnI (detected by MAb 4H6) did not change in the TG hearts compared with the WT control,

the level of WT cTnI decreased in the TG hearts (detected by the TnI-1 blot). The Western blot using anti-cardiac troponin T (TnT) MAb CT3 (3) showed no change in cardiac TnT. MHC, myosin heavy chain. *C*: densitometry quantification confirmed the decreased level of WT cTnI in the TG hearts due to the replacement by cTnI-R193H. Data are means ± SE. $*P < 0.05$, $n = 3$ mice in each group.

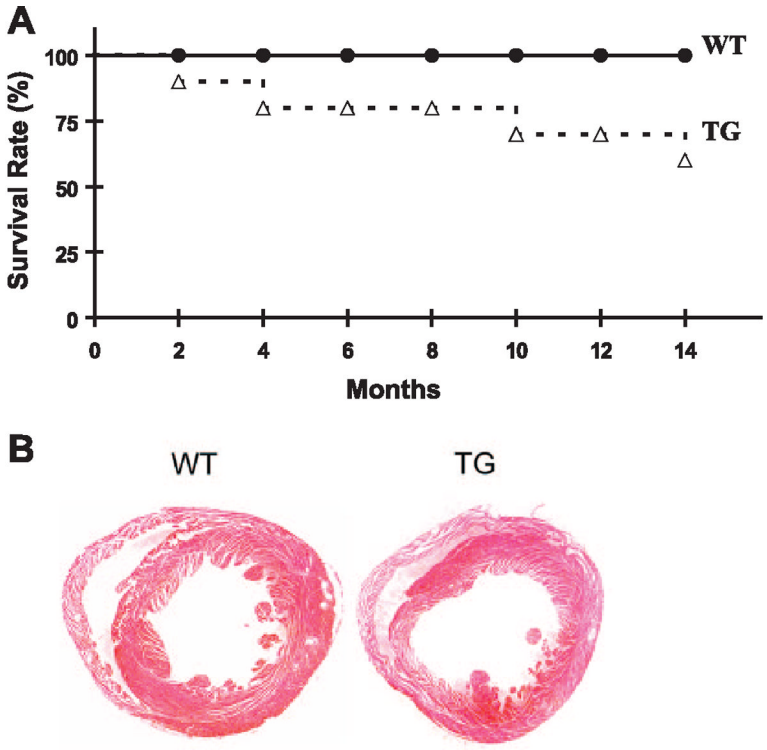

Fig. 2.

Mortality rate and cardiac histological examination in TG and WT mice. *A*: mortality rate was recorded in 15 WT and 15 TG mice until the age of 14 mo. *B*: hematoxylin and eosin staining in cardiac histological sections in TG and WT mice at age of 10 mo did not show any significant hypertrophy or ventricular dilation.

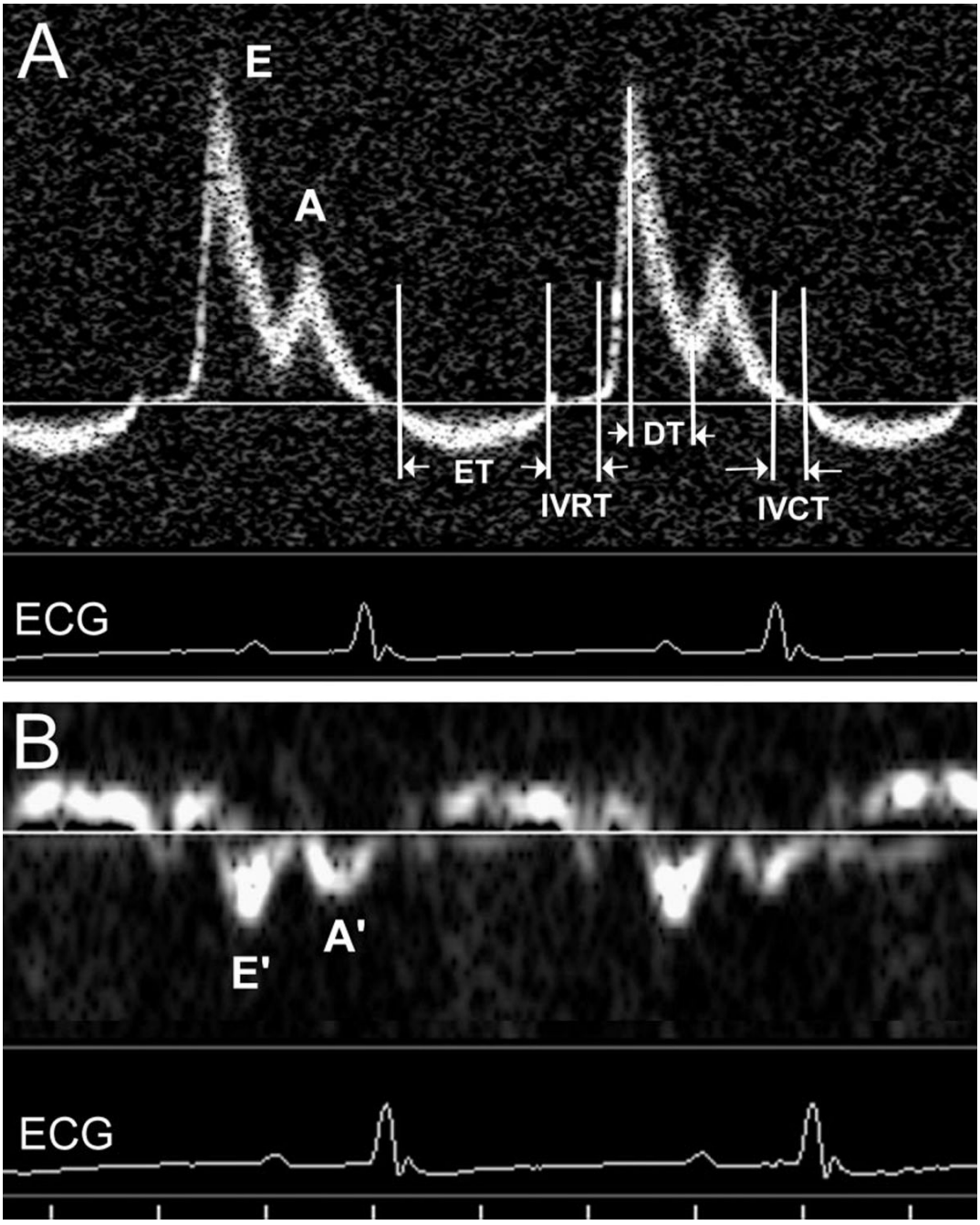

Fig. 3.

Typical mitral inflow pattern (*A*) and mitral annulus velocity pattern (*B*) obtained with Doppler-echocardiography from WT mice. E, E wave indicating early ventricular filling; A, A wave indicating late filling caused by atrial contraction; ET, ejection time; IVRT, isovolumetric relaxation time; DT, deceleration time; IVCT, isovolumetric contraction time; E′, peak E′ velocity in Doppler tissue imaging (DTI); A′, peak A′ velocity in DTI.

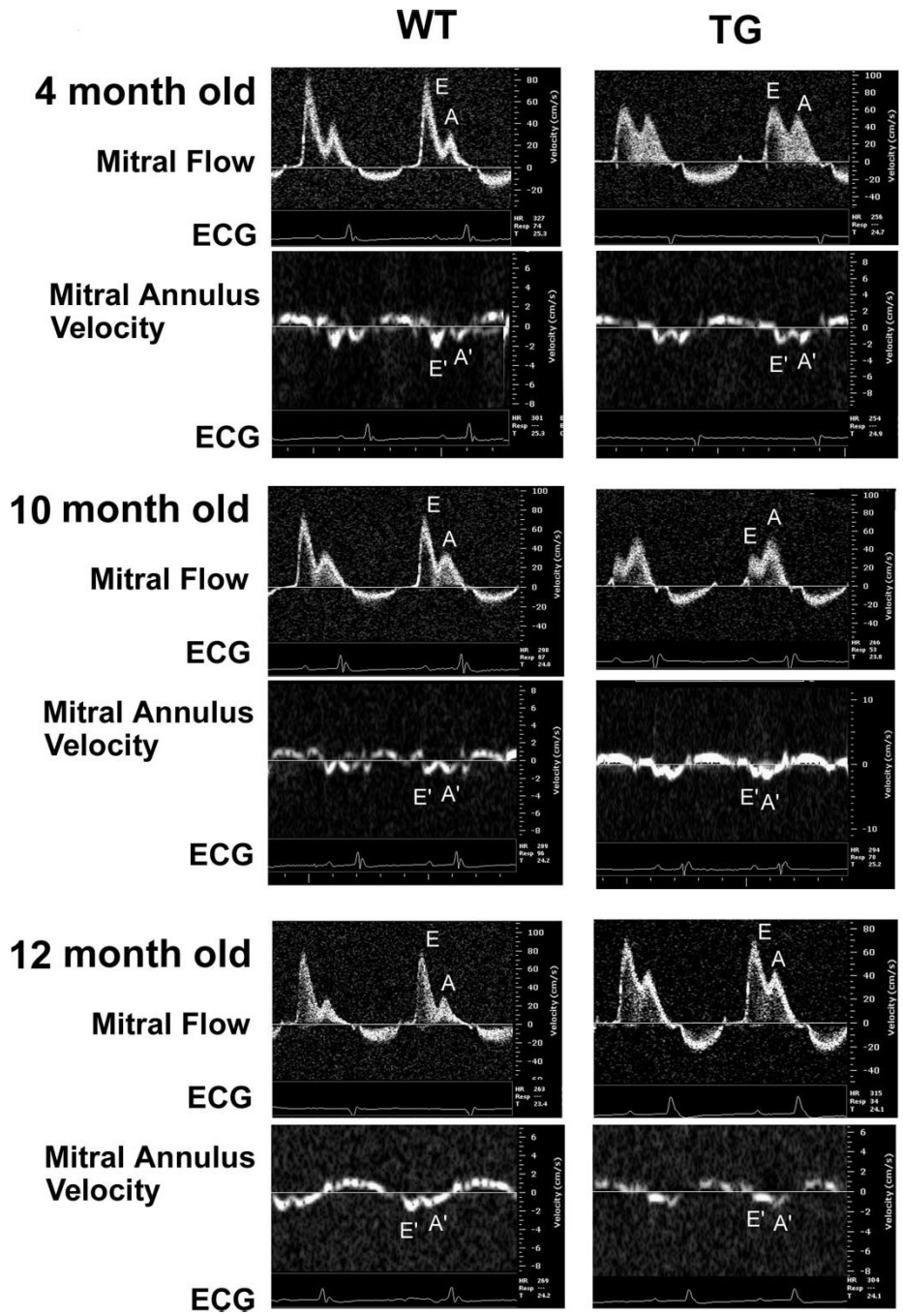

Fig. 4.

Doppler echo-ECG imaging from WT and TG mice. Typical mitral inflow pattern and mitral annulus velocity pattern observed in WT and TG mice at the age of 4 mo (*top*), 10 mo (*middle*), and 12 mo (*bottom*). E-to-A ratio and E′-to-A′ ratio reversals were observed in TG mice at the age of 10 mo, and decreased E′ and A′ velocity were observed in TG mice at the age of 12 mo; 6 WT and 6 TG mice were investigated in each group.

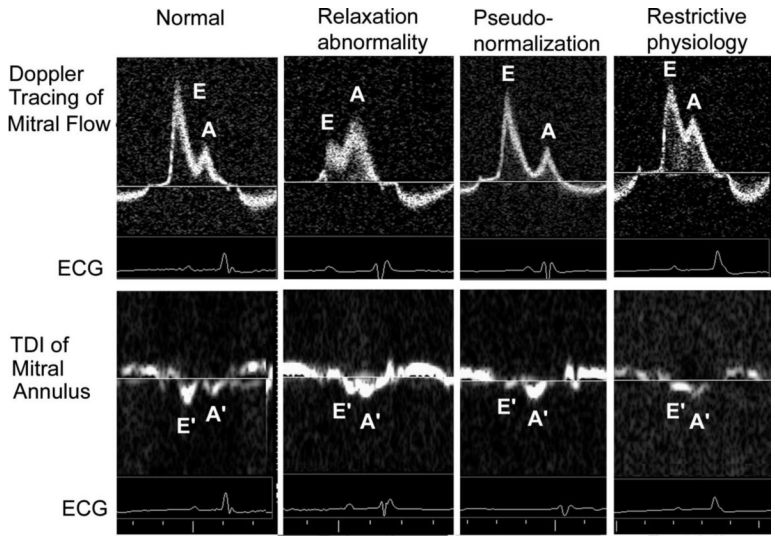

Fig. 5.

General patterns of mitral inflow and mitral annulus velocity observed from normal to restrictive physiology in TG mice. TDI, tissue-Doppler imaging.

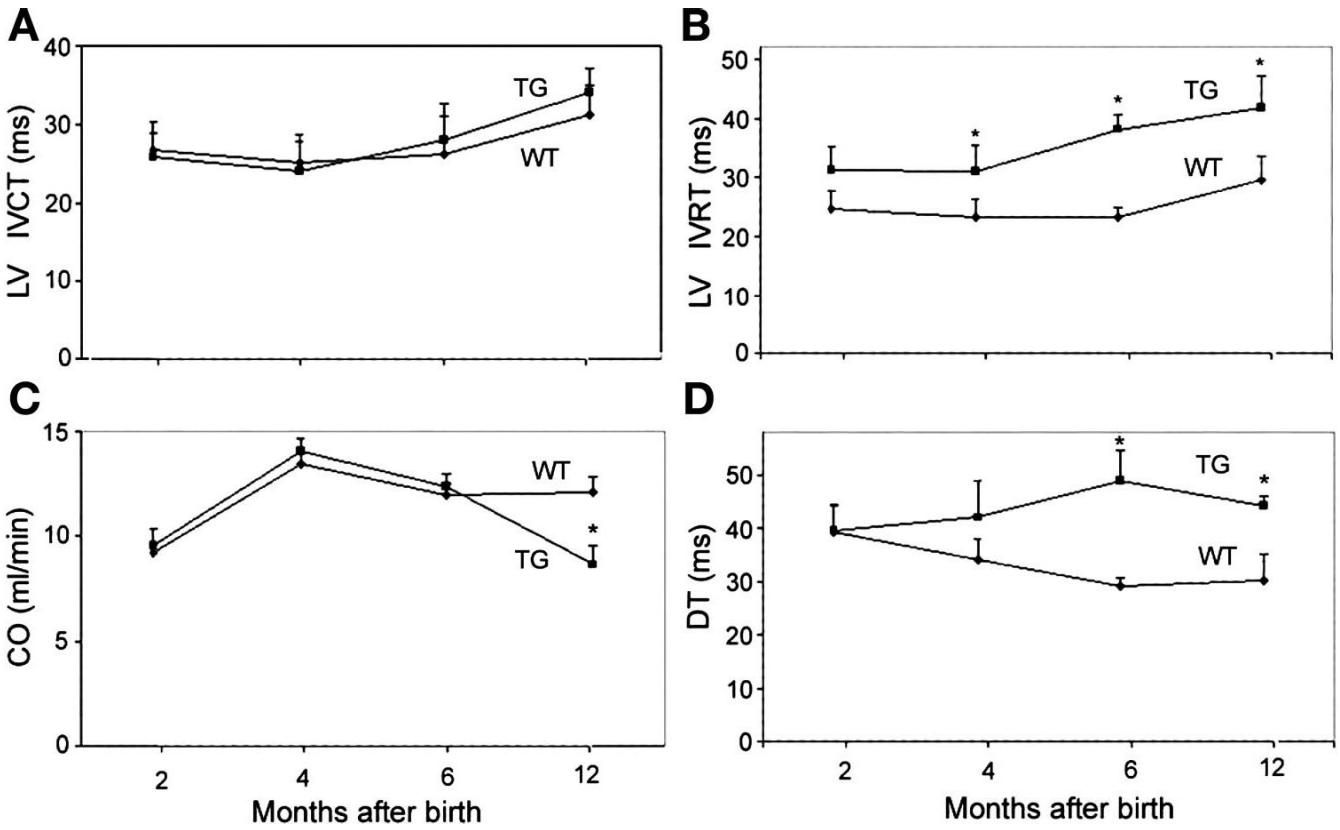

Fig. 6.

Summary of Doppler echocardiography measurements of mitral inflow patterns and left ventricular (LV) diastolic function in WT and TG mice. *A*: LV IVCT measured by mitral impulse Doppler represents a contraction function of the LV. *B*: LV IVRT measured by mitral impulse Doppler represents a diastolic function of the LV. IVCT and IVRT measurements were performed as illustrated in Fig. 3. Three to five cardiac cycles were averaged for each experimental animal. *C*: cardiac output (CO) measurement in TG and WT mice indicates that CO deceased significantly in TG mice at age of 12 mo. *D*: early wave DT represents an early ventricular rapid filling rate. Data are means ± SE from 6 mice per group. **P* < 0.05.

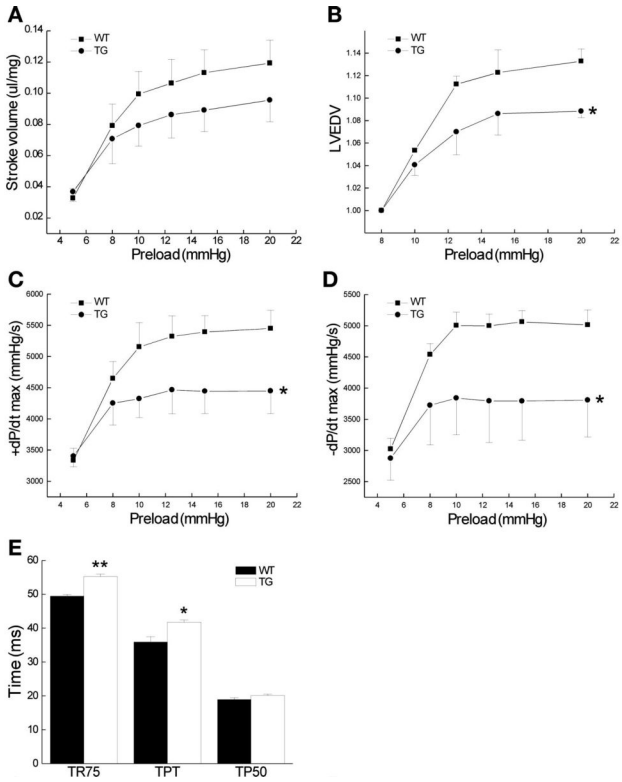

Fig. 7.

Cardiac function measured in isolated working heart preparations. Isolated working heart function was measured at 90-mmHg afterload and preloads of 5, 8, 10, 12.5, 15 and 20 mmHg. *A*: decrease in the stroke volume of the TG hearts normalized by heart weight compared with the WT controls. *B*: reduced response of the LV end-diastolic volume (LVEDV) in the TG hearts to the increases in preload. *C* and *D*: maximum velocity of LV pressure development ($\pm dP/dt_{max}$). These velocity changes are consistent with changes in duration of the contractile and relaxation phases shown in *E*. Data are means ± SE. **P* < 0.05, ***P* < 0.01 by independent *t*-test. *n* = 3 for each group.

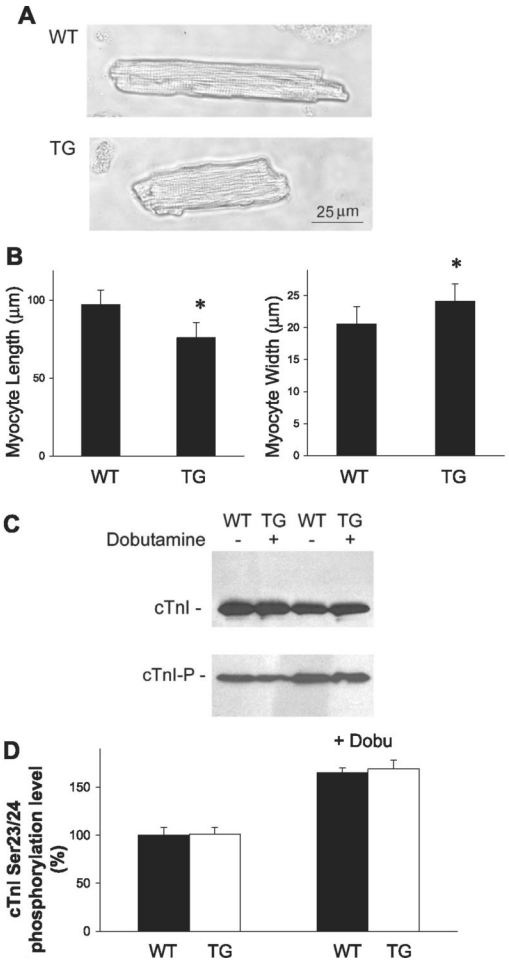

Fig. 8.

Myocyte morphology and cTnI Ser23/24 phosphorylation in TG mice. *A*: representative bright-field images (×40) of WT cardiac myocyte and cTnI^{193His} myocyte. Scale bar, 25 μm. *B*: summary of average length and width of cardiac myocytes from 10-mo-old WT or cTnI^{193His} mouse hearts. Data are means ± SE from 200 WT myocytes and 200 cTnI^{193His} myocytes. *$P < 0.05$. *C*: phosphorylation levels at cTnI Ser23/24 (cTnI-P) were detected by Western blotting in 10-mo-old WT and cTnI^{193His} cardiac myocytes without or with dobutamine treatment. Cardiac protein samples were separated on 4–12% gradient gel. cTnI concentrations were detected with anti-cTnI antibodies to be the controls for equal protein sample loading. *D*: summary of cTnI Ser23/24 phosphorylation level in WT and TG hearts in the absence or presence of dobutamine. Data are averages from 3 separate experiments. The phosphorylation level in WT mouse heart in the absence of dobutamine treatment is used as the control (100%).

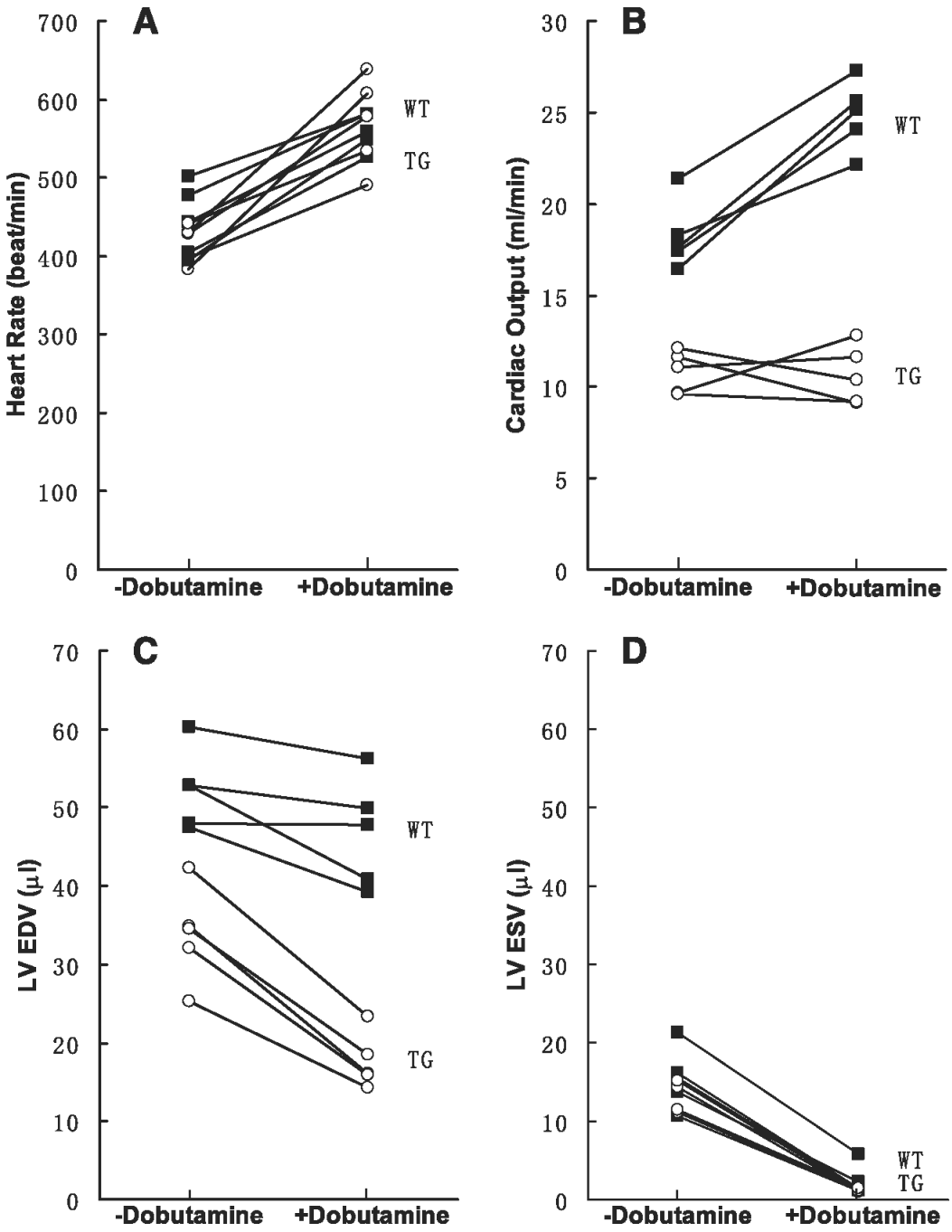

Fig. 9.

Cardiac responses in WT and TG mice to dobutamine stimulation. Dobutamine was given intraperitoneally at 1.5 μg/g body wt, and heart rate (*A*), CO (*B*), LVEDV (*C*), and LV end-systolic volume (LVESV) (*D*) before and after dobutamine administration were plotted individually for 5 WT and 5 TG mice.

Table 1

Doppler-echocardiography data from cTnl transgenic and wild type mice

Parameters	2 mo		4 mo		6 mo		12 mo	
	WT	cTnI^{193His}	WT	cTnI^{193His}	WT	cTnI^{193His}	WT	cTnI^{193His}
Body weight, g	21.3±0.6	23.0±1.0	35.3±1.5	35.5±1.8	39.0±1.0	41.3±1.2	48.9±9.0	42.0±5.0
Heart weight, mg							213.7±12.3	209.6±16.3
HW/BW, mg/g							4.45±0.28	4.73±0.24
Heart rate, beats/min	421±27	444±23	474±24	487±120	457±16	452±25	469±23	421±19
Echo-ECG								
End-diastolic LV PW, mm	0.98±0.1	0.92±0.1	0.97±0.2	0.97±0.3	1.01±0.2	0.99±0.1	1.02±0.1	1.01±0.2
End-systolic LV PW, mm	1.19±0.2	1.21±0.2	1.18±0.1	1.20±0.2	1.14±0.2	1.17±0.1	1.16±0.2	1.17±0.3
LVEDD, mm	4.05±0.2	3.34±0.4*	4.11±0.3	3.44±0.3*	4.22±0.4	3.12±0.5*	4.18±0.2	3.11±0.3*
LVESD, mm	2.87±0.1	2.21±0.2	2.97±0.2	2.31±0.2	2.88±0.2	2.28±0.1	2.90±0.2	2.67±0.4
LV EF, %	61.5±5.2	58.4±4.3	60.3±4.8	59.1±5.8	59.3±4.1	57.1±3.4	58.4±4.1	39.5±5.1*
Mitral Doppler								
E velocity, mm/s	500±54	711±98	638±162	595±106	642±78	765±26	761±42	669±67
A velocity, mm/s	377±47	418±104	360±30	500±59	484±128	569±72	511±142	439±106
E/A	1.3±0.1	1.8±0.4	1.8±0.3	1.2±0.1	1.4±0.2	1.4±0.1	2.3±0.98	1.6±0.53
DTI								
E′ velocity, mm/s	21.2±0.7	20.9±3.4	19.5±6.3	17.8±3.2	16.8±0.9	21.6±2.7	25.7±4.9	12.6±2.1
A′ velocity, mm/s	15.0±0.4	17.1±1.5	12.7±3.0	16.1±2.9	13.9±1.8	17.8±3.3	19.0±4.6	15.0±1.8
E′/A′	1.5±0.1	1.2±0.1	1.5±0.2	1.1±0.6	1.2±0.1	1.2±0.2	1.4±0.1	0.8±0.1*

Values are means ± SD from 5 wild-type (WT) and 5 cardiac troponin I (cTnI)^{193His} mice at each time point from 2 to 12 mo of age. HW, heart weight; BW, body weight; LV, left ventricle; PW, posterior wall thickness; LVEDD, LV end-diastolic dimension; LVESD, LV end-systolic dimension; EF, ejection fraction; DTI, Doppler tissue imaging.

*$P < 0.05$, significant difference between measurements in cTnI^{193His} mice compared with WT littermates at the same age.